Supporting document: Viscous flow through high permeability channels in a layered porous medium

A. Rathore, Z. Zheng, and C. K. Sahu

We provide supportive information here on the manuscript entitled "Viscous flow through high permeability channels in a layered porous medium." This document includes brief descriptions on additional experiments performed in a three-layer symmetric packed-bead system, with both permeable and impermeable walls to mimic the flows in unconfined and confined media, respectively.

I. ADDITIONAL LABORATORY EXPERIMENTS

We have performed additional laboratory experiments with the aim of further verifying some of the findings of §2 from the manuscript. Compared with the experiments described in §2 of the manuscript, these additional experiments were performed in a three-layer symmetric packed-bead system to reduce the boundary effects at the walls. We also increased the permeability contrast between the beads layers. In addition, these experiments were performed in two different tanks separately to investigate the effects of unconfined and confined boundaries, which are depicted in figure 1. Specifically, panel a is for the unconfined medium and panel b for the confined medium. The experimental tank in figure 1a for the unconfined case were meshed (and hence had holes) at the sidewalls, and the complete tank was submerged in a larger tank filled with salt water of same density as in the experimental tank, ensuring a fully saturated medium. In this way the setup allowed a controlled boundary condition and replicated a fully saturated environment for the experiment.

Parameters	Experiment (Permeable wall)	Experiment (Impermeable wall)
Layer thickness (H) (cm)	$w = 3$, $H_2 = 13.5$	$w = 3$, $H_2 = 11$
Beads diameter (d) (cm)	$d_1 = 0.32 \pm 0.02$, $d_2 = 0.13 \pm 0.02$	$d_1 = 0.5 \pm 0.02$, $d_2 = 0.05 \pm 0.02$
Porosity (ϕ)	$\phi_1 = \phi_2 = 0.40$	$\phi_1 = 0.39$, $\phi_2 = 0.40$
Permeability (k) (cm^2)	$k_1 = 1.04 \times 10^{-4}$, $k_2 = 1.54 \times 10^{-5}$	$k_1 = 5.99 \times 10^{-4}$, $k_2 = 2.83 \times 10^{-6}$

TABLE I: Values of the parameters shown in figure 1.

Experiment No.	Δh (cm)	Glycerin (%)	Water (%)	μ_1 mPa.s	ρ_1 (g/cm^3)	Salt (%)	μ_2 mPa·s	ρ_2 (g/cm^3)	Δp ($\times 10^2$ Pa)
EXP-1 (Permeable wall)	24.5	100	0	780	1.26	30	1	1.21	30.34
EXP-2 (Permeable wall)	49.5	100	0	780	1.26	30	1	1.21	61.24
EXP-3 (Impermeable wall)	68	100	0	570	1.25	30	1	1.21	83.4
EXP-4 (Impermeable wall)	68	100	0	780	1.26	30	1	1.21	84.3

TABLE II: Details of the experiments performed. $()_1$ = injected fluid, $()_2$ = ambient fluid. Note: The fluid viscosity is measured by viscometers and its variation is primarily due to different room temperatures during experiments performed.

A. Experimental set-up

We employ two transparent acrylic tanks of dimensions 30 cm × 30 cm × 2 cm and 112 cm × 25 cm × 2 cm for the experiments in unconfined and confined media, respectively, as shown in figure 1. The tanks were filled with spherical glass beads of diameters d_1 and d_2 to make distinct layers of different permeability. The higher permeability layer with larger beads had width w and the low permeability layers had width H. The values of w and H for both

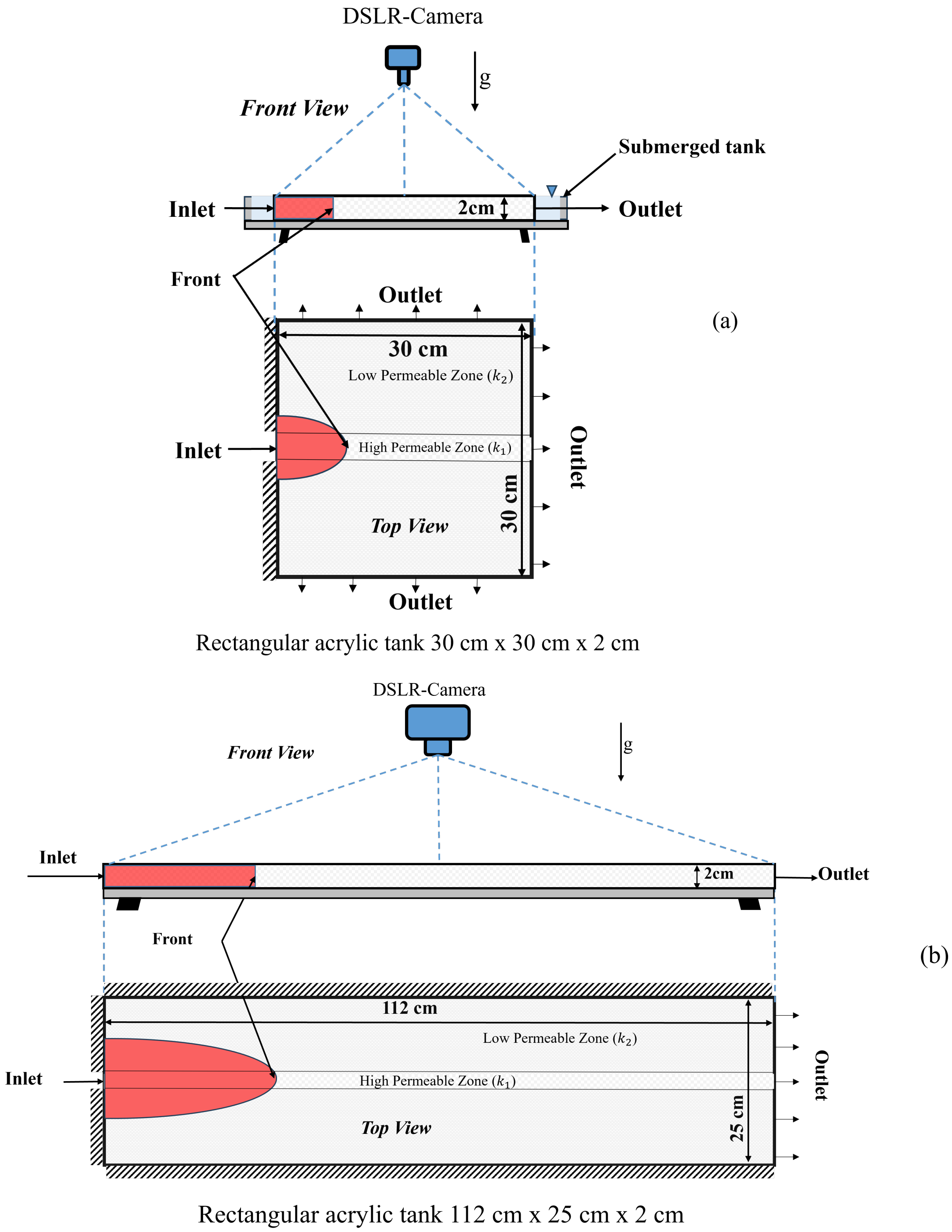

FIG. 1: Schematic of the experimental setups: Fluid injection into (a) an unconfined porous medium (with permeable walls), and (b) a confined porous medium (with impermeable walls).

setups are given in table I. The porosity and permeability were measured in the same way as described in the main manuscript for the original experiments, and their values in each cases for the current experiments are detailed in table I. The mesh used in the case of unconfined medium to make the permeable walls was made of nylon and had the thickness of 1 mm and pore size of 0.5 mm. The complete tank was saturated with salt water of density ρ_2 and viscosity μ_2. For these experiments, pure glycerin was used as the more viscous fluid for injection, which had density ρ_1 and viscosity μ_1. The properties of the ambient and injected fluids are listed in table II for various experiments.

The viscous fluid was injected into the experimental tank through the high permeability layer, using an overhead

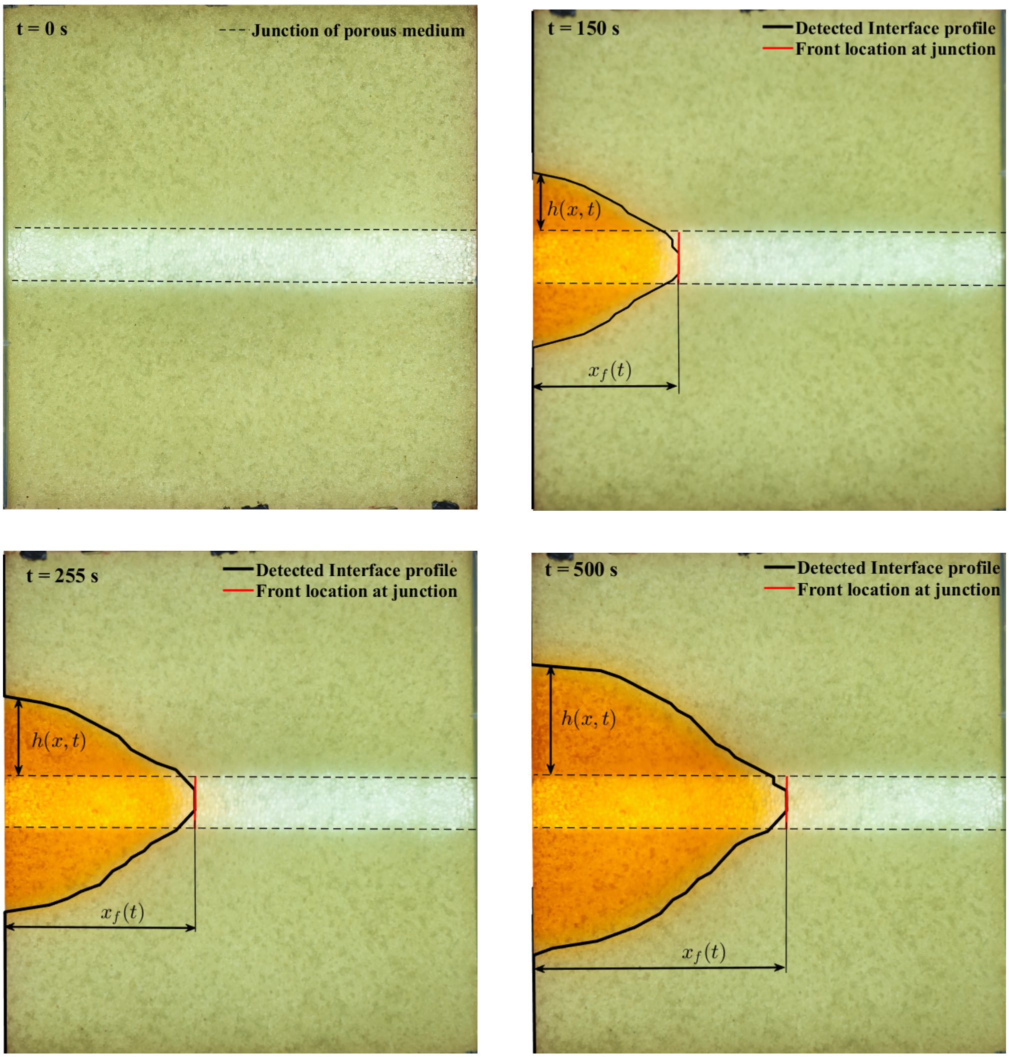

FIG. 2: Representative experimental images for Exp-1 of flow in an unconfined porous medium at four different times: (a) $t = 0$ s, (b) $t = 155$ s, (c) $t = 255$ s, and (d) $t = 500$ s. The black curves in the images represent the fluid-fluid interface.

tank that maintained the inflow. Both the overhead tank and the outlet of the experimental tank were open to the atmosphere. Moreover, during an experimental run, the glycerin level in the overhead tank was maintained constant using an overflow hole. Thus, the elevation difference Δh between the overhead tank and the experimental tank outlet created a constant hydrostatic pressure difference of $\Delta p = (\rho_1 - \rho_a)g\Delta h$ for the inflow during each experiment. The elevation of the overhead tank was varied between different sets of experiments. We performed a total of four additional experiments in this symmetric packed-bead system. More details of the experiments are listed in table II. For flow visualization, image processing and data extraction, we used the same dye calibration technique and Matlab algorithm as described in the main manuscript.

B. Experimental observations

Figures 2 and 3 illustrate the time evolution of the propagating front $x_f(t)$ and thickness profile $h_f(x,t)$ using the solid black curves in different panels for these additional experiments in unconfined and confined media at representative times, respectively. The junction of the two permeable layers is highlighted using a dashed black line. We observe that the experiments shown in figure 2 for the displacement flow in the unconfined medium qualitatively match better with the theory. The experiment in figure 3 seems to be under the influence of significant boundary effects of the impermeable walls.

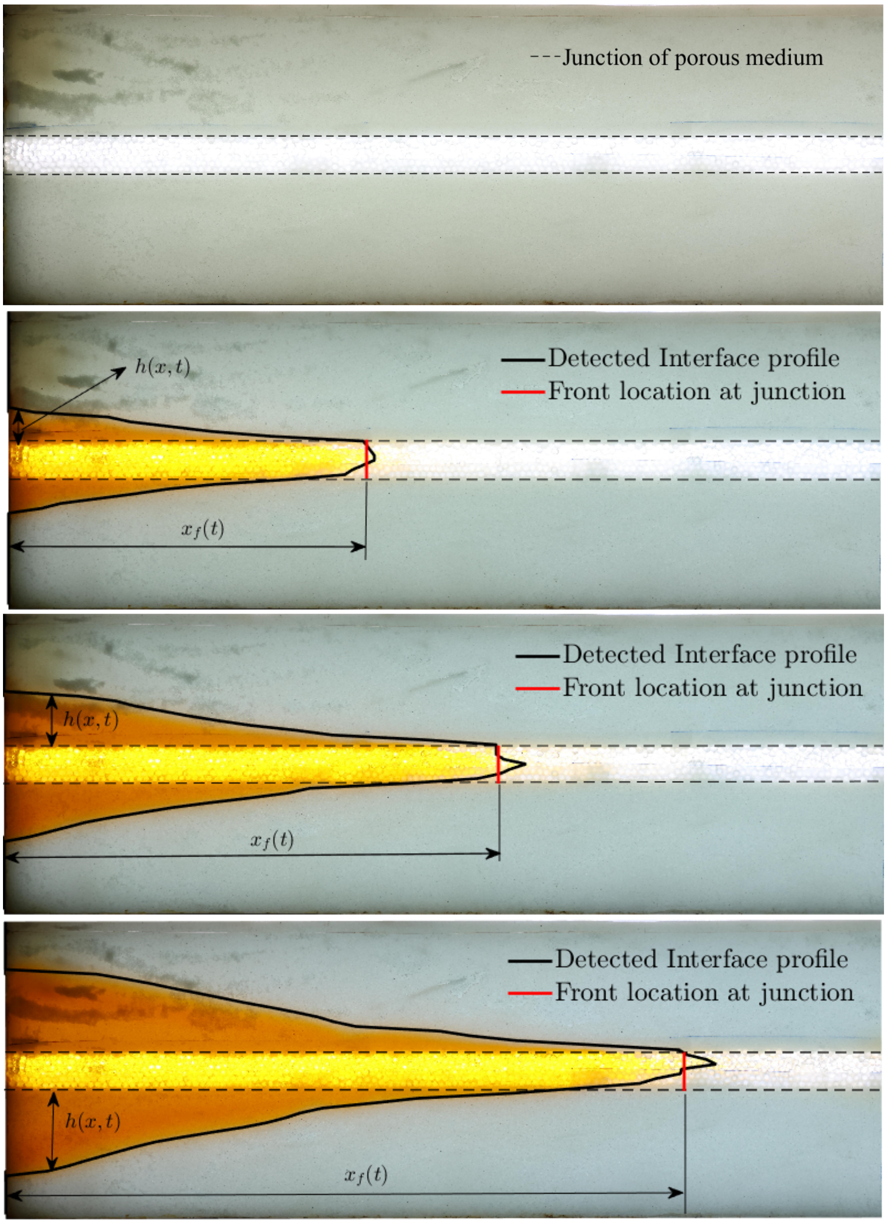

FIG. 3: Representative experimental images for Exp-3 of flow in a confined porous medium at four different times: (a) $t = 0$ s, (b) $t = 105$ s, (c) $t = 210$ s, and (d) $t = 435$ s. The black curves in the images represent the fluid-fluid interface.

In figures 4 and 5, we present images from all four experiments at a fixed time of 450 s. We observe different degrees of profile stretching in the high permeability layer, depending on the experimental conditions. Notably, compared with the original experiments in the main text, the invading fluid in these additional experiments is less stretched in the high permeability layer, and the frontal location $x_f(t)$ is better defined. The reasonably flat fronts in these images are consistent with the theoretical model. Note that the details of the experiments are given in table II, where all experiments have the viscosity ratio of around 780, except that in Exp-3 with impermeable wall the viscosity ratio is only around 570. In all cases, we observe much less significant longitudinal stretching of the interface profile in the high permeability layer, compared with the experiments reported in the main text.

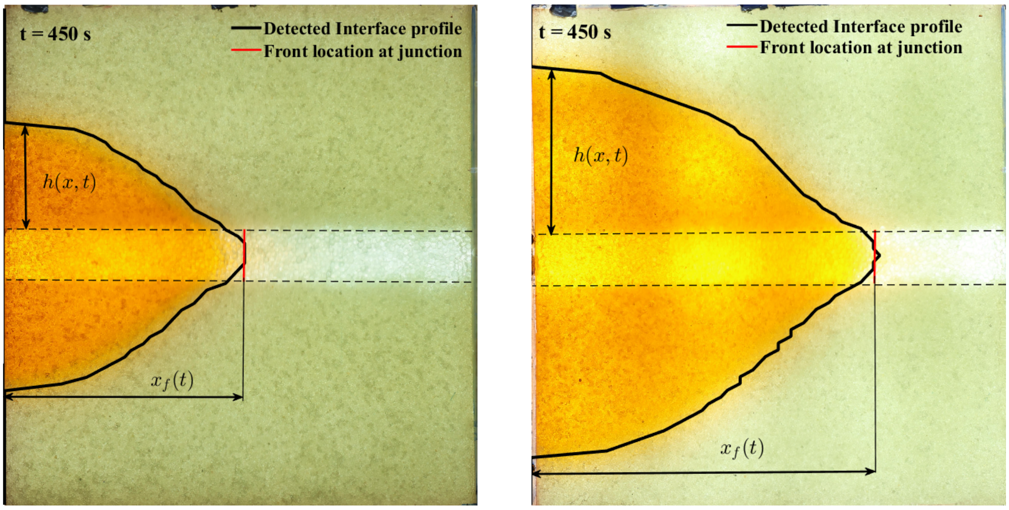

FIG. 4: Comparison of the two experiments of fluid displacement in an unconfined porous medium at the same time $t = 450$ s: (a) Exp-1 with $\Delta h = 24.5$ cm and $\mu_2/\mu_1 = 780$, (b) Exp-2 with $\Delta h = 49.5$ cm and $\mu_2/\mu_1 = 780$. The primary difference is the inlet pressure of the injecting fluids.

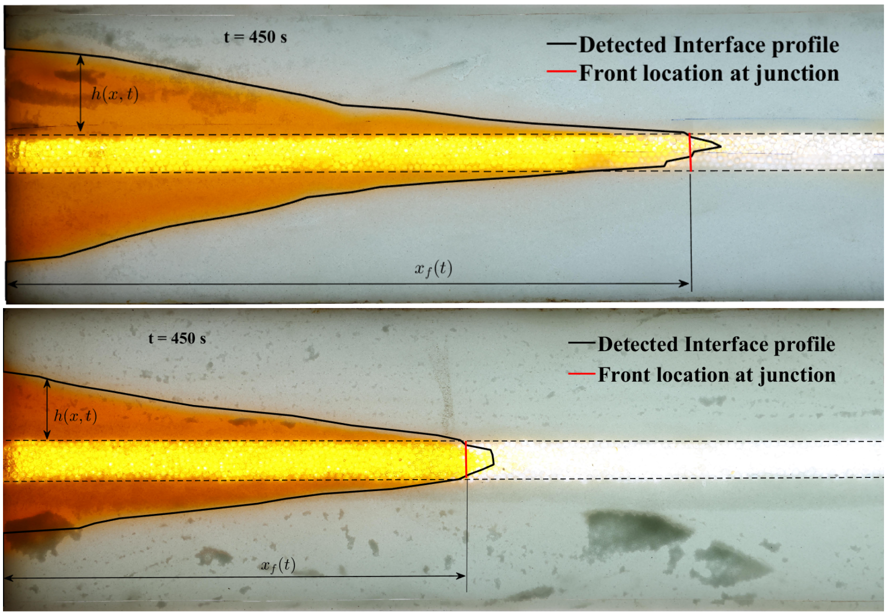

FIG. 5: Comparison of the two experiments of fluid displacement in a confined porous medium at the same time $t = 450$ s: (a) Exp-3 with $\Delta h = 68$ cm and $\mu_2/\mu_1 = 570$, (b) Exp-4 with $\Delta h = 68$ cm and $\mu_2/\mu_1 = 780$. The primary difference is the viscosity of the injecting fluids.

II. COMPARISON BETWEEN THEORY AND EXPERIMENTS

In this section, we compare the experimental measurements for the experiments in table II of this document with the theoretical predictions in §2 of the main manuscript. In particular, we focus on the location of the propagating front $x_f(t)$ in the high permeability layer and the thickness profile $h(x,t)$ of the fluid-fluid interface in the low permeability layer.

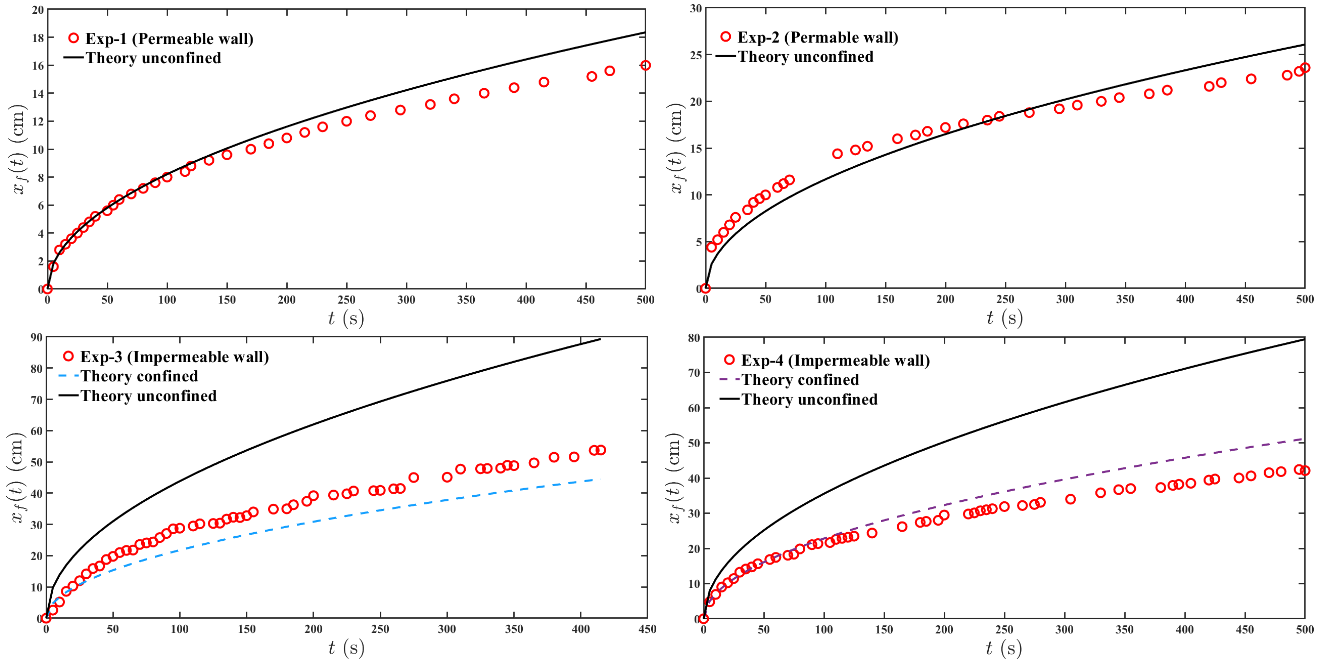

FIG. 6: Time evolution of the frontal location $x_f(t)$ in the unconfined porous medium with permeable side walls: (a) EXP-1, and (b) EXP-2, and in the confined porous medium with impermeable side walls: (c) EXP-3, and (d) EXP-4. Theoretical predictions of the unconfined theory are also included as the solid black curves.

	Front propagation (x_f)				**Maximum profile thickness** (h_0)			
Experiment	**MARE (%)**	**RMSE**	**StdDev**	**StdErr**	**MARE (%)**	**RMSE**	**StdDev**	**StdErr**
EXP-1 (Permeable wall)	7.51	1.21	0.69	0.07	3.89	0.30	0.30	0.04
EXP-2 (Permeable wall)	8.82	1.79	1.80	0.19	7.30	0.80	0.41	0.05
EXP-3 (Impermeable wall)	19.44	7.08	2.53	0.28	23.51	1.14	0.76	0.08
EXP-4 (Impermeable wall)	12.46	5.03	2.84	0.28	23.75	1.09	0.30	0.03

TABLE III: Comparison of MARE, RMSE, StdDev, and StdErr values for front propagation and maximum profile thickness for the data shown in figures 6–7. The calculations for EXP-3 and EXP-4 are based on the confined theory.

A. Frontal location

In figure 6 the theoretical prediction for the propagating front $x_f(t)$ from the main manuscript is compared with the experimental results of this supporting document. Similarly, figure 7 compares the results of the profile thickness $h(0,t)$ at $x = 0$ versus time t. We observe that the agreement in figures 6a-6b and 7a-7b for the displacement process in unconfined porous media are much more promising.

These comparisons are further quantified by calculating mean errors between the theory and experiments for the data points included in these figures. To find the mean errors, we first find absolute errors between the theory and experiment at various specified times and then average the values to find the mean error for the given experiment. The Mean absolute relative error (MARE), root mean square error (RMSE), standard deviation (StdDev), and standard error (StdErr) for all experiments for both $x_f(t)$ and $h(0,t)$ are listed in table III and IV. These calculations support the major observations that the simple model works well for displacement flows in unconfined porous media.

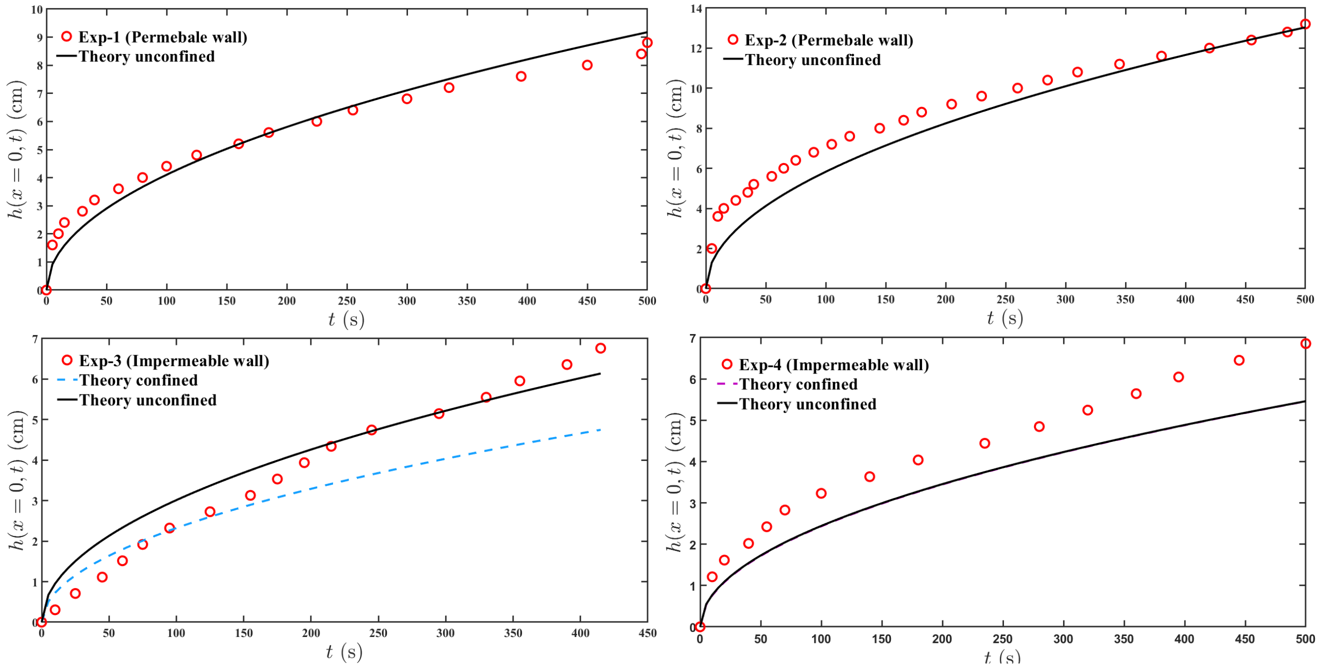

FIG. 7: Time evolution of the maximum profile thickness $h(0,t)$ at $x=0$ for displacement flow in the unconfined porous medium with permeable side walls: (a) EXP-1, and (b) EXP-2, and in in the confined porous medium with impermeable side walls: (a) EXP-3, and (b) EXP-4. Theoretical predictions of the unconfined theory are also included as the solid black curves.

Experiment	**MARE (%)**	**RMSE**	**StdDev**	**StdErr**
EXP-1 (Permeable wall)	4.06	0.34	0.32	0.04
EXP-2 (Permeable wall)	8.23	0.80	0.41	0.05
EXP-3 (Impermeable wall)	41.01	0.89	0.83	0.22
EXP-4 (Impermeable wall)	19.02	0.09	0.04	0.01

TABLE IV: MARE, RMSE, StdDev, and StdErr values for thickness profile $h(x,t)$ for all four experiments based on the data shown in figure 8. The calculations for EXP-3 and EXP-4 are based on the confined theory.

B. Profile shape

In figure 8, we present a comparison for the interface profile $h(x,t)$ of the invading fluid in the low permeability layer for the last image of each experiment, i.e. at time t_{max}. The curves in the figure are normalized using $x_f(t_{max})$ and $h(0,t_{max})$ for individual experiments such that all experiments can be compared together. The theoretical thickness profiles are plotted for both unconfined and confined porous media, predicted for various viscosity and inlet pressure conditions. We find a good agreement in figure 8a for the displacement flow in the unconfined case, whereas there are much more significant differences in figure 8b for the displacement flow in the confined media.

As also described in the Appendix of the manuscript, we see over-prediction by the theory across some intermediate regions in the case of experiments in confined media. The profiles obtained from simulations for all cases show good agreements with the experimental results, and slight deviations from the theoretical predictions. The agreements between experiments and numerics are particularly good for the cases involving more viscous fluid injection, e.g., for Exp-1, Exp-2 and Exp-4. This agreement is consistent with what we observe in figure 6 for the propagating front in the high permeability layer and figure 7 for profile thickness at $x=0$ in the low permeability layer. In the experiments with higher viscosity, the mismatch is less significant for the frontal location estimation.

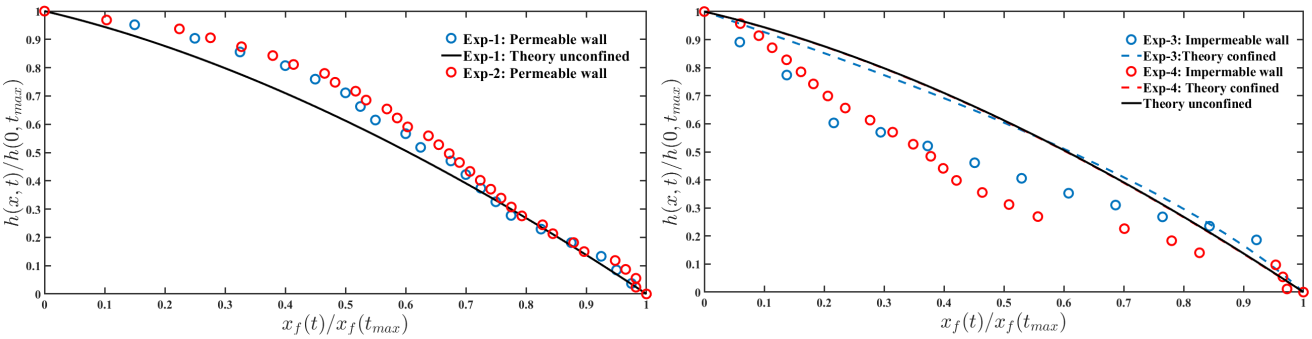

FIG. 8: The normalised profile shapes of the fluid-fluid interface with respect to the maximum values $h(0, t_{max})$ of thickness profile at $x = 0$ and front location $x_f(t_{max})$ at the final time t_{max} for all fluid displacement experiments in both the (a) unconfined and (b) confined porous media. Solid curves represent the theoretical predictions provided in the main manuscript for the unconfined medium, whereas the dashed curve are for the confined medium presented in the appendix of the main document.

III. FINAL REMARKS

To further illustrate the fluid displacement process, we have designed and performed four additional laboratory experiments in two three-layer symmetric packed-bead porous systems of the sandwich type. These additional experiments helped us understand the influence of permeable and impermeable boundaries in the far field, and how they could affect the application of the simple theory described in the main text.

In particular, when comparing the theoretical predictions (as described in the main text) with the experimental observations, we found that the normalised profile shapes at different times collapse reasonably well. We particularly see a much better match in case of experimental results for fluid displacement processes in unconfined porous media with permeable side walls. The universal profile shape aligns reasonably well with the theoretical predictions. But in contrast, when the side walls are made impermeable, the influence of flow confinement becomes important, and the theoretical predictions of the one-dimensional models described in the main text become much worse.

Meanwhile, with these additional experiments performed, we are allowed understand more about the generation of the stretched tail in the high permeability layer. Our current understanding is that the stretched tail of the injecting fluid in the main manuscript in the high permeability layer is influenced by boundary effects at the wall (which leads to a thin gap that is much more permeable for fluid flow), and the impermeable packing (which leads to a mixed bead layer at the junction of intermediate permeability). In the additional symmetric experimental setup of the sandwich type with three bead layers, much less significant stretching is observed in the high permeability layer. Additionally, the injection method, which uses a point source rather than a line source across the high-permeable layer, differs from the assumptions in the theoretical model. Such a difference could possibly lead to two-dimensional flow effects in the high permeability layer that can not be predicted by the one-dimensional models.

To close this document, we conclude that the simple theory described in the main text has successfully captured several major trends observed in the experiments, and hence provides a reasonable representation of the underlying physical processes, in particular, for the displacement process in the unconfined porous medium. In the future, it may also be of use to construct a regime diagram (based on two-dimensional numerical simulations and/or additional experiments) to indicate when the simple model provides the best predictions. Solving the problem in its dimensionless form would also be helpful.